INTERFACE

rsif.royalsocietypublishing.org

Research

Cite this article: Murienne BJ, Chen ML, Quigley HA, Nguyen TD. 2016 The contribution of glycosaminoglycans to the mechanical behaviour of the posterior human sclera. *J. R. Soc. Interface* **13**: 20160367.
http://dx.doi.org/10.1098/rsif.2016.0367

Received: 11 May 2016
Accepted: 6 June 2016

Subject Category:
Life Sciences–Engineering interface

Subject Areas:
biomechanics

Keywords:
sclera, glycosaminoglycans, chondroitinase ABC, mechanical testing, glaucoma, myopia

Author for correspondence:
Barbara J. Murienne
e-mail: barbara.murienne@gmail.com

The contribution of glycosaminoglycans to the mechanical behaviour of the posterior human sclera

Barbara J. Murienne[1], Michelle L. Chen[1], Harry A. Quigley[2] and Thao D. Nguyen[1]

[1]Department of Mechanical Engineering, Johns Hopkins University, Baltimore, MD, USA
[2]Glaucoma Center of Excellence, Johns Hopkins University School of Medicine, Baltimore, MD, USA

BJM, 0000-0003-1841-8803

We characterized the structural and mechanical changes after experimental digestion of sulfated glycosaminoglycans (s-GAGs) in the human posterior sclera, using ultrasound thickness measurements and an inflation test with three-dimensional digital image correlation (3D-DIC). Each scleral specimen was first incubated in a buffer solution to return to full hydration, inflation tested, treated in a buffer solution with chondroitinase ABC (ChABC), then inflation tested again. After each test series, the thickness of eight locations was measured. After enzymatic treatment, the average scleral thickness decreased by 13.3% ($p < 0.001$) and there was a stiffer overall stress–strain response ($p < 0.05$). The stress–strain response showed a statistically significant increase in the low-pressure stiffness, high-pressure stiffness and hysteresis. Thus, s-GAGs play a measurable role in the mechanical behaviour of the posterior human sclera.

1. Introduction

The mechanical properties of the sclera have been shown to play an important role in the initiation and development of ocular diseases such as glaucoma and myopia in both experimental and modelling analyses. Glaucoma is the second leading cause of blindness worldwide [1] and is characterized by an 'excavation' of the tissues of the optic nerve head (ONH) [2], as well as the dysfunction [3,4] and loss [5,6] of the axons of the retinal ganglion cells (RGCs) at the ONH [7]. The intraocular pressure (IOP) can produce a high level of stresses and strains in the tissues of the ONH, depending on the mechanical properties of the sclera. This mechanical insult is potentially responsible for the mechanical failure of the ONH tissues and for damaging the RGC axons directly or through poor vascular nutrition and mechanical activation of astrocytes [8]. These events can occur at any level of IOP, whether higher or lower than that found in non-glaucoma eyes [8–11]. Myopia is a common refractive error often characterized by the axial elongation of the eye wall [12]. Patients with high myopia are at increased risk for several blinding diseases, such as macular degeneration [13] and glaucoma [14]. Elongation of the sclera occurs by remodelling of the extracellular matrix structure and is accompanied by significant changes in the mechanical properties of the sclera.

The tensile and viscoelastic behaviour of the posterior sclera is altered in glaucoma and myopia. The peripapillary sclera of human glaucomatous eyes has a lower creep rate and higher stiffness compared with that of normal eyes in inflation tests [15]. In a monkey model of glaucoma, the posterior sclera also exhibits a higher stiffness under inflation [16] and the peripapillary sclera shows a higher equilibrium modulus after stress relaxation following a rapid deformation, but no change in the time-dependent parameters compared with that of normal eyes in uniaxial strip tests [17]. The posterior sclera of human myopic eyes reaches a higher strain at maximum pressure than that of normal eyes under uniaxial testing [18]. In a tree shrew model of myopia, the posterior sclera also

THE ROYAL SOCIETY PUBLISHING

shows a greater strain at maximum pressure [19–21], as well as a higher creep rate [20,22], but a similar stiffness [19,22] than those of normal eyes, in uniaxial strip tests.

Collagen represents 80% of the dry weight of the sclera [23], whereas elastin fibres and proteoglycan (PG) core proteins represent 2% of its dry weight [24,25]. In comparison, GAGs represent only 0.5–1% of the scleral dry weight [26]. GAGs are assemblies of disaccharide units into chains of various lengths, most of them attached to a core protein to form PGs. The most abundant GAGs in the posterior sclera are chondroitin sulfates and dermatan sulfates [27,28]. GAGs attract and retain water through their negative ionic charges [29], as well as their osmotic pressure [30–32]. They also directly interact with collagen fibrils [33–36] through electrostatic interactions [33,37] and have been hypothesized to regulate collagen fibril spacing through hydration (swelling) [32,38,39], GAG–GAG charge repulsion [40] and GAG–GAG anti-parallel interactions [41].

The changes in the mechanical properties of the posterior sclera are associated with specific changes in the collagen and elastin structure in glaucoma [42–45] and myopia [46–48]. In addition, alterations in the s-GAG content have also been reported in glaucoma and myopia. There is currently no data on the change in GAG content in the posterior sclera in glaucoma. However, a higher s-GAG content was reported in the iris [49] and lamina cribrosa [50] of human glaucomatous eyes, which was consistent with the findings of studies on animal models of glaucoma [51,52]. A decrease in the overall GAG content was found in the posterior sclera of human myopic eyes [18], which was consistent with the results obtained with animal models of myopia [47].

The mechanical role of GAGs remains debated in the literature. The effect of GAG degradation is tissue-dependent and inconsistent results have even been reported for the same tissue, probably due to differences among species and differences in testing protocol. Studies have measured changes in the viscoelastic behaviour of cartilage [53], aorta [54] and heart valve leaflets [55] following GAG removal, while others have observed no change in the viscoelasticity of ligaments [56,57]. The stiffness increased with GAG digestion in arteries [58], lungs [59], as well as ligaments [60] and aorta [54] in the small strain range (i.e. toe region). GAG degradation decreased the stiffness of the aorta in the high strain range (i.e. linear region) [54], but did not affect the stiffness of cartilage [53], tendons [61] and ligaments in a different study [56]. We recently studied the effect of s-GAG removal on the mechanical behaviour of the posterior porcine sclera [62]. s-GAG degradation with ChABC from a hydrated state significantly decreased the scleral stiffness at low pressures (i.e. toe region), the hysteresis and the final creep rate, while increasing the stiffness at high pressures (i.e. linear region) and the strain at the onset of strain stiffening (i.e. length of the toe region). The changes were found to be opposite to the changes observed for an increase in hydration from a baseline (control) to a hydrated state. In addition, differences in the inflation response between the meridional and circumferential directions were significantly reduced after enzymatic s-GAG degradation. These changes in the tensile and viscoelastic behaviour showed that s-GAGs play an important role in the mechanical behaviour of the posterior porcine sclera. Specifically, the observed findings were interpreted to exceed the effects of hydration alone and suggested an interactive effect on the collagen fibrils.

In this study, we performed inflation testing of the posterior human sclera after incubation in buffer alone and after treatment in buffer containing ChABC to degrade the s-GAGs. We compared the inflation behaviour for each specimen before and after treatment with ChABC. The results were used to evaluate whether s-GAG degradation induced changes in the mechanical response of the posterior human sclera and whether the changes in humans were comparable to those measured in our prior study on pigs [62]. The findings were interpreted for their significance to the mechanical and pathological contribution of s-GAGs to the scleral mechanical behaviour in glaucoma and myopia.

Table 1. Number of specimens used for s-GAG quantification, hydration measurement, mechanical testing and thickness measurements. 1/1 indicates that one eye was used from one donor, 9/5 indicates that nine eyes were used from five donors, asterisk denotes that both eyes were from the same pair and hash denotes that the same eyes were used for both experiments.

	no. of specimens
s-GAG quantification	$n = 1^{*}/1$
hydration measurement	$n = 1^{*}/1$
mechanical testing	$n = 9^{\#}/5$
thickness measurement	$n = 9^{\#}/5$

2. Material and methods

2.1. Specimens and glycosaminoglycan degradation

Eleven human donor eyes were obtained from the National Disease Research Interchange (NDRI) from six donors with an average age of 74.0 ± 9 years, whose medical records show no history of glaucoma (table 1). The medical records did not provide information about myopia. All structural and mechanical outcomes were measured in the four anatomical quadrants of the posterior scleral shell (superior-nasal (SN), superior-temporal (ST), inferior-nasal (IN) and inferior-temporal (IT)), outside the peripapillary region. To confirm the effectiveness of our s-GAG degradation protocol developed for pigs [62] in the human sclera, we first determined the s-GAG content, in micrograms per milligram of wet tissue weight, of two samples taken in each of the four quadrants of a single eye. Both samples from each quadrant were divided into two experimental groups (figure 2). In the first group, the specimens were incubated for 18 h at 37°C in a modified Trizma buffer at pH 8.0 (buffer-treated). In the second group, the specimens were incubated for 18 h at 37°C in Trizma buffer containing ChABC (C2905, Sigma-Aldrich, St Louis, MO, USA) at 2 units ml^{-1} (enzyme-treated). ChABC is known to specifically degrade chondroitin and dermatan sulfates at pH 8.0. We then inferred the s-GAG content in micrograms per milligram of dry tissue weight from hydration measurements on two samples taken in each quadrant of the contralateral eye, and each one incubated in either buffer alone or buffer containing ChABC (figure 2). The remaining nine eyes were inflation tested after incubation for 18 h in buffer alone (buffer-treated) and after subsequent incubation for 18 h in the enzyme solution (enzyme-treated). Scleral thicknesses were measured at the end of each inflation test. We confirm that our research followed the tenets of the Declaration of Helsinki.

2.2. Specimen preparation

The eyes were received in a closed container, on a gauze pad soaked with saline solution to reduce dehydration and used within 48 h *post-mortem*. The extraocular fat and muscles were

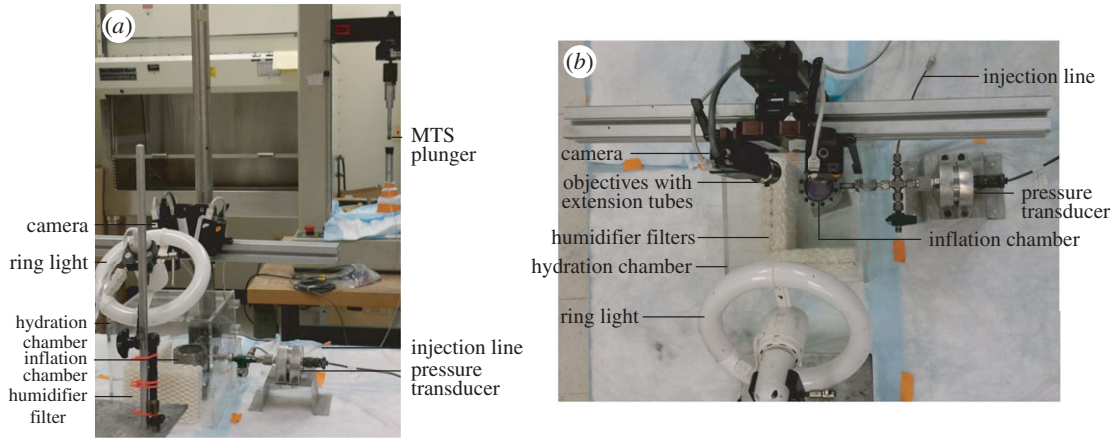

Figure 1. (*a*) Side view and (*b*) top view of the experimental set-up showing the inflation chamber, pressure transducer, MTS, hydration chamber, as well as the imaging and lighting systems. (Online version in colour.)

removed, leaving a clean scleral surface. For two eyes, we used a 8 mm biopsy punch to excise samples from each quadrant for s-GAG quantification and hydration measurements (figure 2). The samples were punched 2 mm away from the ONH and away from visible arteries and veins. Two 3×3 mm square samples were then cut from each disc, from which we gently removed the retina and choroid (figure 2).

The eyes used for mechanical testing and thickness measurements were glued to a custom-made acrylic holder centred about the ONH using cyanoacrylate (Permabond 910, Electron Microscopy Sciences, Hatfield, PA, USA) (figure 3*a*). The anterior sclera was cut away and the intraocular structures, including the retina and choroid, were removed from the remaining posterior scleral shell.

2.3. Glycosaminoglycan quantification and hydration measurement

The protocol for s-GAG content quantification was previously described [62]. Briefly, the s-GAG content was assessed on 3×3 mm samples, taken in each of the four quadrants of a single eye (figure 2) and subjected to either buffer-treatment or enzyme-treatment, using the Blyscan assay (Accurate Chemical & Scientific Corporation, Westbury, NY, USA). The samples were first blotted dry on Whatman paper for 1 min, weighed wet and incubated in a solution of Papain (P3125, Sigma-Aldrich, St Louis, MO, USA) for 18 h at 60°C, following Boubriak *et al*. protocol [63]. The s-GAG content per dry tissue weight in each quadrant was inferred using hydration measurements of the wet over dry sample weight ratio. The wet sample weight was measured after blotting the samples dry on Whatman paper for 1 min using a precision balance (XP26DR, Mettler-Toledo LLC, Columbus, OH, USA). The wet samples were weighed inside pre-weighed eppendorf tubes to prevent further evaporation. The samples were then dehydrated by incubation for 48 hours in an oven at 60°C and weighed in the same manner.

2.4. Mechanical testing

For inflation testing, the specimens that were glued to the custom plastic holder were then clamped to a custom inflation chamber (figure 1*a*,*b*). Dulbecco's phosphate-buffered saline (DPBS) was injected into the chamber using an MTS-actuated syringe (MTS, Eden Prairie, MN, USA) (figure 1*a*). The pressure inside the chamber was monitored using a pressure transducer (TJE, 2 psig range, Honeywell, Morristown, NJ, USA) and fed back into the MTS testing machine to control the motion of the MTS crosshead using a PID controller (figure 1*a*,*b*). The specimens were first equilibrated at the baseline pressure 0.21 kPa for 30 min, then subjected to a load–unload cycle from baseline pressure to 6 kPa at 0.13 kPa s^{-1}, followed by a 30 min recovery period at baseline pressure. The baseline pressure was then maintained for the thickness measurements. Preconditioning cycles were not performed. A previous study showed that the effects of preconditioning are negligible for repeated inflation testing of the posterior sclera [15,64]. The inflation chamber was enclosed in a clear Perspex humidity chamber with 90% humidity to prevent dehydration of the specimens during testing (figure 1*a*,*b*).

2.5. Thickness measurement

The scleral thickness was measured at eight locations, two in each of the four quadrants of the eyes (figure 2) using a 15 MHz ultrasound transducer (V260-45, Olympus NDT Inc., Waltham, MA, USA) fitted with a 1.5 mm diameter Sonopen tip (DLP-302, Olympus NDT Inc.), as described in a previous study [62]. The ultrasound transducer was linked to a pulser–receiver (5073PR-15-U, Olympus NDT Inc.) and the echoes from the outer and inner scleral surfaces were recorded from an oscilloscope (TDS220, Tektronix Inc., Beaverton, OR, USA). The scleral thickness T was calculated as

$$T = \frac{1}{2} c_{\text{sclera}} \Delta t, \tag{2.1}$$

where $c_{\text{sclera}} = 1597$ m s^{-1} [65] is the speed of sound in the sclera and Δt is the time difference between the peaks of the outer and inner sclera echoes. The thickness in each quadrant was reported as the average of both measurements.

2.6. Digital image correlation

The posterior sclera was speckled with black India ink (figure 3*a*) using an airbrush (ECL4500 HP-CS, Iwata Medea Inc., Portland, OR, USA) prior to mechanical testing to enhance the contrast for the 3D surface displacement measurements using 3D-DIC. Images were acquired using a stereoscopic system equipped with two monochrome cameras with a 2 megapixel resolution (GRAS-20S4M-C, Point Grey, Richmond, BC, Canada), 26° stereo angle and objectives with a 35 mm focal length (Xenoplan 1.9/35 mm-0901, Schneider Optics, Hauppauge, NY, USA) fitted with 5 mm long extension tubes (54–628, Edmund Optics, Barrington, NJ, USA). Illumination was provided by a circline light bulb (90922 L, Commercial Electric, Cleveland, OH, USA) to increase image contrast and maintain even lighting across the specimen. Images with a 0.018 mm per pixel resolution were captured every 2 s during mechanical testing with Vic-Snap 2009 (Correlated Solutions Inc., Columbia, SC, USA)

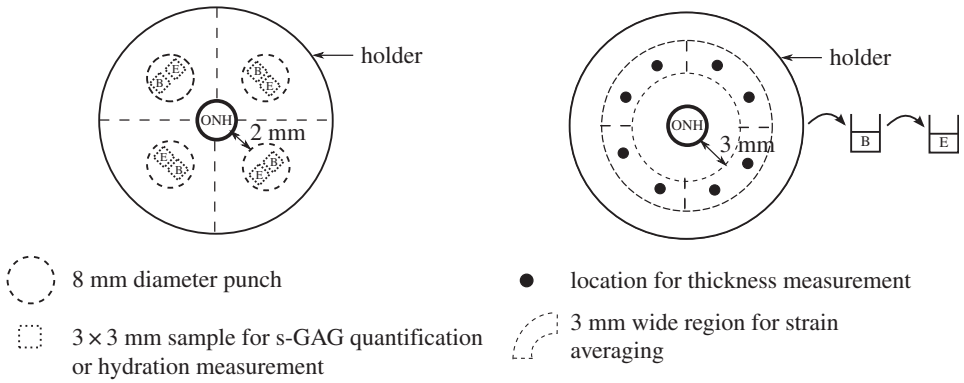

Figure 2. Schematic of the human posterior sclera protruding from the holder showing the ONH as well as the locations of the samples used for the s-GAG quantification and hydration, the locations of the thickness measurements and the regions where the strains were averaged. The letter B indicates the samples incubated in buffer alone, while the letter E indicates samples treated with the enzyme. For the s-GAG quantification and hydration measurement, samples from the same eye were subjected to each condition, while for the mechanical testing the specimens were subsequently treated with the buffer alone and then with the enzyme solution.

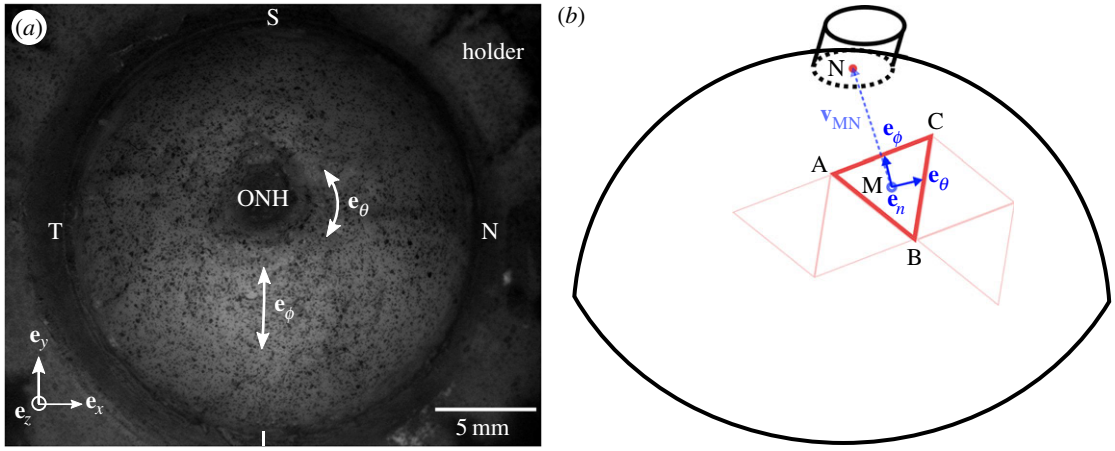

Figure 3. (*a*) Image of a left human scleral shell mounted on a holder and speckled for 3D-DIC tracking, showing the eye anatomical quadrants and directions. (*b*) Schematic showing how the local basis was defined for each Delaunay triangle. For each triangle, the vector $\mathbf{v}_{MN}$ was defined from the centroid of the triangle M to the centre of the ONH base N. This vector was then projected onto the plane of the triangle and normalized to find the meridional direction $\mathbf{e}_\phi$. The circumferential direction $\mathbf{e}_\theta$ was defined as the cross product $\mathbf{e}_\theta \times \mathbf{e}_n$, where $\mathbf{e}_n$ is the outward normal unit vector to the plane of the triangle. (Online version in colour.)

and imported into Vic3D 2012 (Correlated Solutions Inc.) for 3D-DIC analysis.

2.7. Strain calculation

For each correlated point at every pressure increment, 3D-DIC provided the 3D surface displacements (u_x, u_y, u_z), from the reference geometry at the baseline pressure, on a two-dimensional Cartesian grid ($\mathbf{e}_x$, $\mathbf{e}_y$) with a 0.090 mm resolution (figure 3*a*). However, given the geometry of the sclera, strains were calculated along circumferential and meridional directions, $\mathbf{e}_\theta$ and $\mathbf{e}_\phi$, respectively (figure 3*a*,*b*). To define the new circumferential-meridional coordinate system, we identified the centre of the ONH base as the pole. The separation of the ONH region from the scleral region was found by an iterative least-squares fitting process. A sphere was fitted to the reference position of the posterior scleral shell and the points with 3% error from the spherical fit radius were removed until the fitting error converged. The remaining points corresponded to the scleral shell over which the strains were calculated, while the points removed corresponded to the ONH. An oblique cylinder was then fitted to the ONH region to determine the centre of the ONH (figure 3*b*).

Surface strains were calculated over triangular domains formed by three nearest neighbour points with average grid spacing of 0.10 mm, as described in Genovese *et al*. [66]. Triangular domains were constructed using the Delaunay triangulation algorithm in MATLAB and were sufficiently small to be assumed planar. The meridional direction $\mathbf{e}_\phi$ was defined for each triangle by projecting the vector $\mathbf{v}_{MN}$ connecting the triangle centroid M to the ONH centre N onto the plane of the triangular domain. The circumferential direction $\mathbf{e}_\theta$ was calculated as the cross product between the meridional direction and the outward unit normal of the triangular region $\mathbf{e}_n$ calculated from the sides of the triangle $\mathbf{x}_{BA}$ and $\mathbf{x}_{CA}$ (figure 3*b*).

Unit orientation vectors were calculated for the sides of the triangle using the reference positions and transformed to a local spherical coordinate system of the triangle to give ($\mathbf{n}^{sph}_{AB}$, $\mathbf{n}^{sph}_{BC}$, $\mathbf{n}^{sph}_{CA}$) (figure 3*b*). The stretches of the sides of the triangular domain (λ_{AB}, λ_{BC}, λ_{CA}) were calculated using the reference positions and displacement vectors. They were used to calculate the components of the right Cauchy–Green stretch tensor $\mathbf{C}$ using the following system of equations:

$$\begin{cases} (\lambda_{AB})^2 = \mathbf{n}^{sph}_{AB} \cdot \mathbf{C}\mathbf{n}^{sph}_{AB} \\ (\lambda_{BC})^2 = \mathbf{n}^{sph}_{BC} \cdot \mathbf{C}\mathbf{n}^{sph}_{BC} \\ (\lambda_{CA})^2 = \mathbf{n}^{sph}_{CA} \cdot \mathbf{C}\mathbf{n}^{sph}_{CA}, \end{cases} \tag{2.2}$$

where $\mathbf{C}$ has the components

$$C = \begin{bmatrix} C_{\phi\phi} & C_{\phi\theta} \\ C_{\phi\theta} & C_{\theta\theta} \end{bmatrix}. \tag{2.3}$$

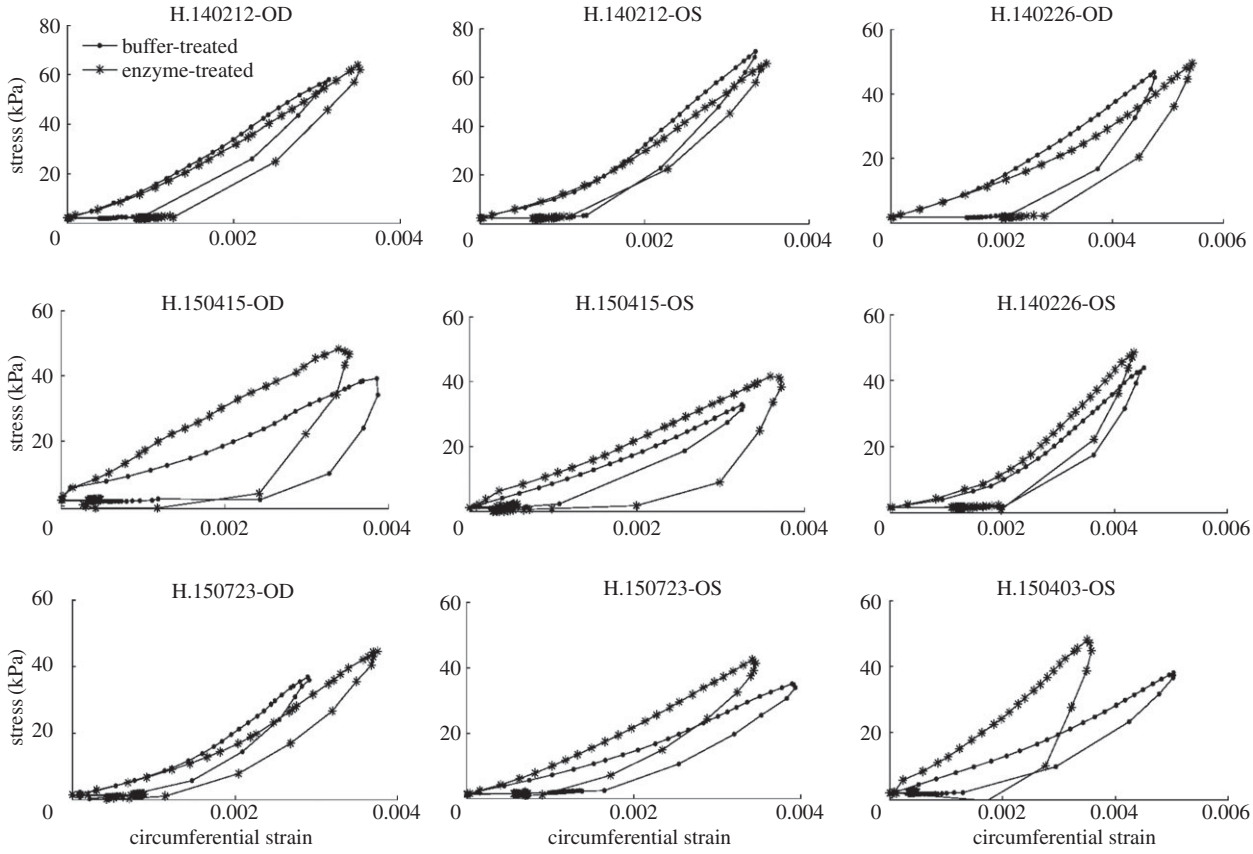

Figure 4. Stress–strain curves in the circumferential direction for all human specimens, averaged over the four anatomical quadrants, after buffer-treatment and after enzyme-treatment. The outliers were locally treated with the MATLAB function *smooth*.

The Green–Lagrange strains in the circumferential and meridional directions were evaluated as $E_{\theta\theta} = 1/2(C_{\theta\theta} - 1)$ and $E_{\phi\phi} = 1/2(C_{\phi\phi} - 1)$. The shear strain was $E_{\phi\theta} = 1/2(C_{\phi\theta})$. The strain components were reported for each quadrant as an average over a 3 mm region in the meridional direction, spanning the entire quadrant and located 3 mm away from the ONH.

2.8. Hoop stress calculation

The hoop stresses $\sigma_{\theta\theta}$ in the circumferential direction and $\sigma_{\phi\phi}$ in the meridional direction were reported at each pressure level for each quadrant as

$$\sigma_{\theta\theta} = \sigma_{\phi\phi} = \frac{Pr}{2T}, \tag{2.4}$$

where P is the pressure, r is the radius of the shell obtained by fitting a sphere to the 3D-DIC reference position data and T is the scleral thickness in a particular quadrant, averaged over two measurements. All three parameters were specific to the specimen treatment state.

2.9. Mechanical data analysis

Four mechanical outcomes were extracted from the stress–strain curves for each scleral shell, quadrant and experimental condition: buffer-treated and enzyme-treated. The low-pressure stiffness was defined as the slope at low pressure calculated by fitting the data points of the loading curves that were within the first 25% of the strain at maximum pressure. The high-pressure stiffness was defined as the slope at high pressure calculated from the fit of the last 30% of the data points of the loading curves. The hysteresis was defined as the area between the loading and unloading curves, calculated by numerical integration using a trapezoidal rule. Outliers were locally treated using the built-in MATLAB function *smooth* with the *rlowess* and *rloess* methods for the loading and unloading curves, respectively. The function *rlowess* performs a local linear interpolation, while *rloess* applies a second-order polynomial local interpolation. Different smoothing methods were used because the loading stress–strain curves for all the specimens were nearly linear, while the unloading curves were significantly more nonlinear (figures 4 and 5). As the loading curves were linear and did not show a clear transition between the toe and linear regions, the strain at maximum pressure rather than the strain at the onset of strain stiffening was extracted as a measure of the tissue extensibility at the maximum pressure.

2.10. Statistical analysis

To evaluate the effect of treatment with the enzyme from a buffer-treated state on the mechanical outcomes and thickness data, we used a repeated measures ANOVA implemented with the built-in MATLAB function *ravova*, using the data for all eyes and quadrants. Repeated measures ANOVA not only indicated whether the mechanical outcomes were different between the experimental groups or between the quadrants, but it also indicated if there was an interaction between group and quadrant. Similarly, we used repeated measures ANOVA to evaluate the difference in mechanical outcomes between the circumferential and meridional directions in both the buffer-treated and enzyme-treated groups.

3. Results

3.1. Glycosaminoglycan content and hydration ratio

The s-GAG content and hydration ratio in all four quadrants of a single eye for samples subjected to either buffer-treatment or enzyme-treatment are shown in tables 2 and 3, respectively. The decrease in s-GAG content after treatment

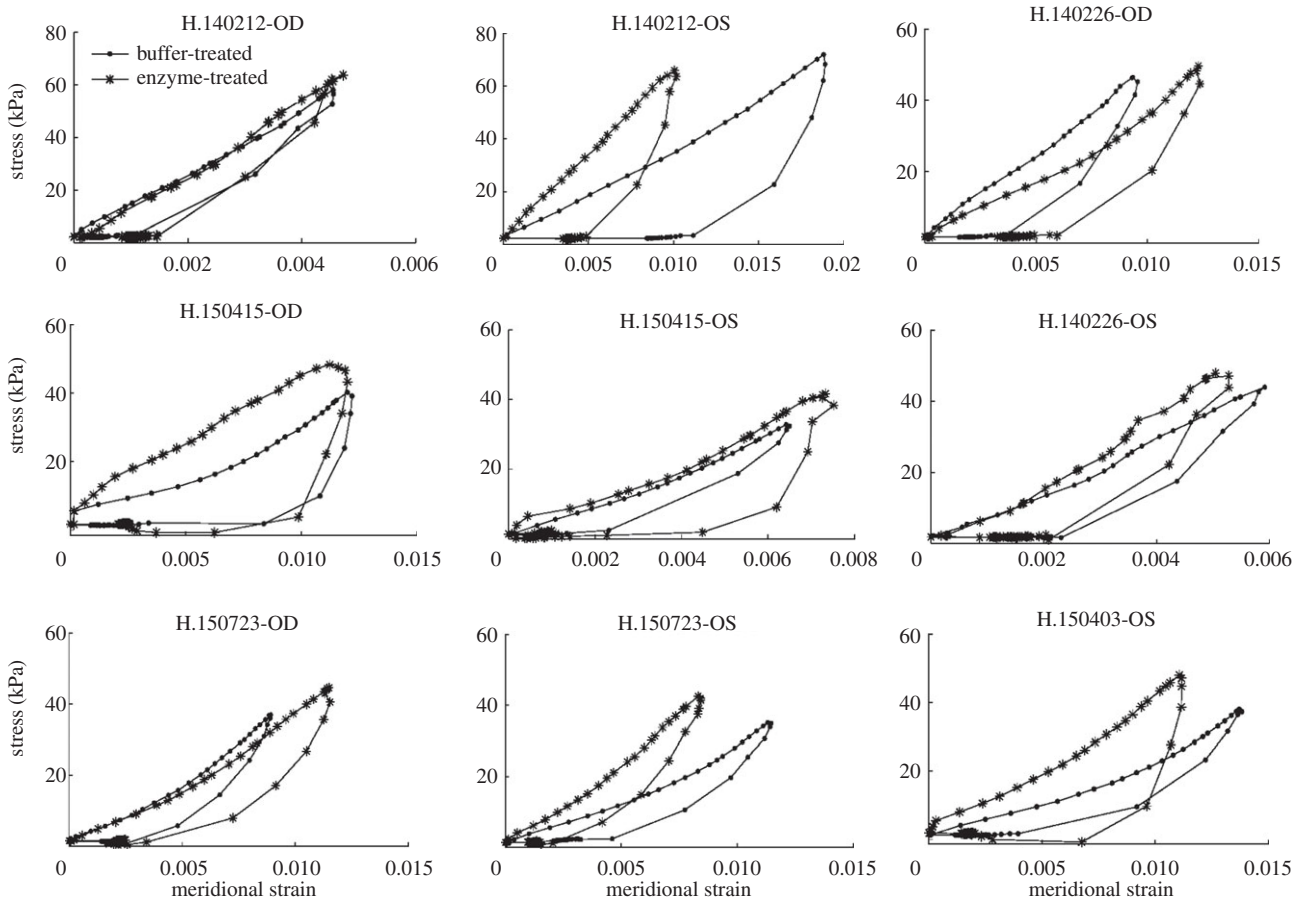

Figure 5. Stress–strain curves in the meridional direction for all human specimens, averaged over the four anatomical quadrants, after buffer-treatment and after enzyme-treatment. The outliers were locally treated with the MATLAB function *smooth*.

Table 2. s-GAG content (μg mg^{-1} dry tissue weight) in each quadrant of a single eye, for samples in the buffer-treated and enzyme-treated groups.

	ST	SN	IT	IN
buffer-treated	5.29	5.87	6.47	3.22
enzyme-treated	0.074	0.066	0.026	0.022

Table 3. Hydration ratio (mg mg^{-1}) in each quadrant of a single eye, for samples in the buffer-treated and enzyme-treated groups.

	ST	SN	IT	IN
buffer-treated	4.204	4.200	4.031	4.029
enzyme-treated	4.186	4.000	4.347	4.031

with the enzyme was more than 98% in all quadrants. No statistics were performed because only one specimen was studied only to confirm the s-GAG degradation protocol previously developed for pig scleras [62] was also effective in humans. The change in hydration after enzyme-treatment obtained for a single eye might not be representative, and therefore was not interpreted in this study.

3.2. Thickness data

The thickness averaged over all eyes and quadrants after treatment with buffer alone and after treatment with enzyme are presented in table 4. The average thickness from the buffer-treated state decreased by 13.3% with enzyme-treatment ($p < 0.001$). There was no interaction between experimental group and quadrant. We did not detect significant spatial differences in the thickness measurements.

Table 4. Thickness (mm) averaged over all specimens and quadrants in the buffer-treated and enzyme-treated groups. Repeated measures ANOVA used for the statistical analysis.

	buffer-treated	enzyme-treated	*p*-value
thickness	0.92 ± 0.26	0.80 ± 0.18	<0.001

3.3. Mechanical behaviour

3.3.1. Comparing the buffer-treated and enzyme-treated groups

Figures 4 and 5 show the stress–strain curves for all human specimens in the circumferential and meridional directions, respectively, after buffer-treatment and after enzyme-treatment. We first compared the mechanical outcomes averaged over the four quadrants and specimens after buffer-treatment and after enzyme-treatment (table 5). In the circumferential direction, treatment with the enzyme from a buffer-treated state increased the low-pressure stiffness by 30.3% ($p < 0.005$), high-pressure stiffness by 11.0% ($p < 0.05$) and hysteresis by 41.6% ($p < 0.001$). In the meridional direction, the low-pressure stiffness increased by 24.2% ($p < 0.05$), the high-pressure stiffness by 11.4% ($p < 0.05$) and the hysteresis by 16.5% ($p = 0.28$) after enzyme-treatment. Treatment with the enzyme had no statistically significant effect on the strain at maximum

Table 5. Comparison of the mechanical outcomes, averaged over all quadrants, between the buffer-treated and enzyme-treated groups, in the circumferential and meridional directions. Repeated measures ANOVA used for the statistical analysis.

	circumferential			meridional		
	buffer-treated	enzyme-treated	*p*-value	buffer-treated	enzyme-treated	*p*-value
low-pressure stiffness (kPa)	7331.1 ± 3478.8	9552.2 ± 5345.2	<0.005	4641.1 ± 3376.0	5763.0 ± 2828.9	<0.05
high-pressure stiffness (kPa)	15 544.2 ± 6172.2	17 254.4 ± 5510.9	<0.05	6819.4 ± 4031.7	7599.1 ± 4739.9	<0.05
hysteresis (kPa)	0.030 ± 0.016	0.043 ± 0.019	<0.001	0.120 ± 0.129	0.140 ± 0.088	0.28
strain at max pressure (mm mm^{-1})	0.0038 ± 9.77 × 10^{-4}	0.0038 ± 8.96 × 10^{-4}	1.0	0.010 ± 0.0046	0.0090 ± 0.0032	0.10

pressure. There was no interaction between experimental group and quadrant for any of the mechanical outcomes. In addition, we did not detect significant spatial differences in any of the mechanical outcomes measured.

3.3.2. Comparing the circumferential and meridional directions

We also compared the difference between the mechanical outcomes in the circumferential and meridional directions, averaged over all specimens and quadrants, after incubation in buffer alone and after incubation with the enzyme. In both the buffer-treated and enzyme-treated groups, the high-pressure stiffness, hysteresis and strain at maximum pressure were significantly different in the circumferential and meridional directions ($p < 0.001$ for all mechanical outcomes and experimental groups). In the buffer-treated group, the circumferential low-pressure stiffness was 58.0% higher and its high-pressure stiffness was 127.9% larger than meridionally. Furthermore, the circumferential strain at maximum pressure was 62.1% smaller and its hysteresis was 74.7% lower than meridionally. These findings were similar in the enzyme-treated group, with the circumferential low-pressure stiffness 65.8% higher, high-pressure stiffness 127.1% larger, strain at maximum pressure 57.6% smaller and hysteresis 69.3% lower than in the meridional direction.

4. Discussion

To better understand the role of s-GAGs in the tensile and viscoelastic properties of the posterior human sclera, we compared its thickness and mechanical behaviour under inflation after buffer hydration with an s-GAG depleted state after treatment with ChABC.

The s-GAG content of the hydrated sclera reported here is similar to that previously reported in the posterior sclera of human eyes [63] and pig eyes [62]. Schultz *et al*. [67] also reported a similar s-GAG content in the posterior sclera of pig and human eyes. The degradation procedure used here for the human sclera removed nearly all s-GAGs, as it had in the porcine sclera. The minimal remaining s-GAGs quantified after enzyme-treatment could represent s-GAGs that are (i) not sensitive to ChABC, such as keratan sulfates, (ii) incompletely degraded but normally sensitive to ChABC or (iii) degraded but incompletely removed from the tissue.

The human scleral thicknesses in this investigation were comparable to those reported in other studies [68,69]. Interestingly, the scleral thickness significantly decreased after enzyme-treatment from a buffer-treated state in human eyes, whereas it increased in pig eyes and was accompanied by an increased hydration as measured in a prior study [62]. The opposite change in scleral thickness following s-GAG degradation between humans and pigs could result from several features of their scleral content. The decrease in thickness in the human sclera after enzyme-treatment could result from an overall loss of water with s-GAG degradation. The amount and type of negative ionic charges determine the scleral capacity for water absorption through charge [29] and osmotic [30–32] effects. However, the water absorption capacity of the tissue is also limited by the collagen interfibrillar spacing, itself governed by GAG–GAG charge repulsion [40] and GAG–GAG anti-parallel interactions [41]. Although the pig and human sclera have a similar s-GAG content as reported in this work and by Schultz *et al*. [67], the s-GAGs remaining in the human sclera after enzyme-treatment might carry fewer negative charges. This could result in a weaker repulsion between the s-GAGs, a decreased interfibrillar spacing and a smaller space for free water to enter the sclera. Enzymatic digestion of chondroitin sulfates was shown to reduce swelling in the cornea [70] and to reduce the 're-expansion' capability of collagen fibrils in dentin upon rehydration [71]. Therefore, the amount of bound water lost after s-GAG removal might not be fully replaced by free water in the human sclera. Additionally, the human sclera has 53% less collagen per dry tissue weight but 1.6 times more collagen non-enzymatic 'glycation-type' cross-links than the pig sclera [67]. This is probably due to the older age of the human donors compared with that of the pigs. A higher collagen cross-link density could lead to a stiffer extracellular matrix, and therefore an increased resistance to swelling and to the intake of more free water. However, Boubriak *et al*. [63] reported no significant decrease in hydration in the hydrated posterior human sclera after s-GAG removal with ChABC, suggesting that a microstructural rearrangement could explain the decrease in thickness measured in the current study. The removal of s-GAG leads to the fusion and thinning of collagen fibrils in cartilage [72] and in decorin and biglycan deficient mice [73,74]. Such microstructural rearrangement could lead to a smaller tissue thickness without necessarily involving a decrease in hydration. Therefore, two processes may underlie the decrease in thickness measured in the human sclera after enzyme-treatment: (i) a lower hydration due to the partial

replacement of the bound water lost after s-GAG digestion by free water and (ii) a microstructure rearrangement such as the fusion or thinning of the collagen fibrils.

Enzyme-treatment from a buffer-treated state increased the low-pressure stiffness, high-pressure stiffness and hysteresis. The combined effect was a statistically significantly stiffer mechanical response of the posterior sclera after s-GAG degradation, though the effect was modest. The increased low-pressure stiffness could be due to a lower hydration and/or the fusion of the collagen fibrils following the loss of s-GAGs, which would be consistent with the observed decreased in thickness. The increased high-pressure stiffness could be explained by a lower tissue hydration and/or an increased free versus bound water in the tissue, which might contribute to a higher friction between the collagen fibrils that are not kept apart by the s-GAGs and their associated water anymore. It may also arise from the fusion of the collagen fibrils. The reason for the increased hysteresis after s-GAG removal remains unclear. It could be due to an increased flow-induced viscosity of the additional free water in the tissue and/or an increased network viscosity despite the loss of s-GAGs. More structural studies are needed to explain this result.

Comparing the mechanical results between pigs [62] and humans, the human sclera was significantly stiffer than the porcine sclera under inflation, which agreed with uniaxial strip tests [67] and is consistent with the higher number of non-enzymatic collagen cross-links in the human sclera [67]. The overall effect of s-GAG degradation was to make the scleral inflation response slightly stiffer in humans, whereas the same treatment dramatically reduced the stiffness of the porcine sclera. In addition, compared with the pig sclera, s-GAG digestion in the human sclera did not change the strain at maximum pressure or difference in the mechanical behaviour between the circumferential and meridional directions, suggesting no alteration to the fibril crimp morphology or anisotropy of the collagen fibrils or of their connections, respectively. This could be due to the abundance of non-enzymatic cross-links in the human sclera. Therefore, differences in the s-GAG degradation effects observed between humans and pigs could be attributed to differences in their scleral collagen cross-link structure and s-GAG types.

The results presented here are not consistent with the reduction in the scleral GAG content [47] and overall more compliant response of the posterior sclera measured in experimental myopia [19–21] and in pigs [62]. Compared to the studies on experimental myopia and pig eyes following s-GAG depletion, this study tested the posterior sclera from elderly donors rather than young animals. Ageing might change the scleral tissue, especially through the addition of non-enzymatic cross-links, in such a way that the tissue softening due to s-GAG degradation is inhibited. This might explain why the results surprisingly follow the same trend as the overall stiffer mechanical behaviour measured in human [15] and experimental [16] glaucoma. Interestingly, another study on human myopic eyes showed an increased strain at maximum pressure and a decreased GAG content compared with normal eyes [18]. This increased scleral compliance could be due to the younger eyes tested compared with those in this study. Therefore, the biomechanical effects of s-GAG degradation may depend on age and hence, on the microstructure of the scleral tissue.

There were several limitations of this study. Mechanical testing and hydration measurement before and after enzyme-treatment could not be performed on the same eyes, hence the lack of hydration data. In addition, we were testing eyes *post-mortem*. They were received at various times after death and, while in humidified jars, their hydration state surely varied. We chose to test them after re-hydration and cannot know their true hydration *in vivo*. Finally, the small strains that we identified would only have found large regional differences, therefore preventing regional mechanical comparisons.

5. Conclusion

In conclusion, nearly complete s-GAG digestion of the human posterior sclera decreased its thickness and led to a small, significant increase in the overall stiffness and hysteresis of the scleral inflation response. While others have reported minimal effects of GAGs on the tensile or viscoelastic mechanical behaviour of connective tissue, we found that s-GAGs play a measurable role in the mechanical behaviour of the posterior human sclera. s-GAGs most likely contribute to the scleral mechanical behaviour through their effects on hydration and collagen–collagen interaction, but their effects may depend on age and therefore tissue microstructure.

Authors' contributions. B.J.M. led the study design and developed the experimental protocols. She performed the s-GAG quantification and hydration measurements, and participated in the inflation and thickness measurements. B.J.M. also wrote the manuscript and discussed the results. M.L.C. developed the strain calculation, performed the statistical analysis, and participated in the inflation and thickness measurements. H.A.Q. and T.D.N. participated in the study design, interpretation of the findings, and the editing of the manuscript.

Competing interests. We declare we have no competing interests.

Funding. This work was supported by the NIH, grant no. EY021500-01 and the NSF Career Award CMMI-1253453.

References

1. Resnikoff S, Pascolini D, Etya'ale D, Kocur I, Pararajasegaram R, Pokharel GP, Mariotti SP. 2004 Global data on visual impairment in the year 2002. *Bull. World Health Organ.* **82**, 844–851.
2. Quigley HA, Hohman RM, Addicks EM, Massof RW, Green WR. 1983 Morphologic changes in the lamina cribrosa correlated with neural loss in open-angle glaucoma. *Am. J. Ophthalmol.* **95**, 673–691. (doi:10.1016/0002-9394(83)90389-6)
3. Quigley HA, Anderson DR. 1976 The dynamics and location of axonal transport blockade by acute intraocular pressure elevation in primate optic nerve. *Invest. Ophthalmol. Vis. Sci.* **15**, 606–616.
4. Minckler D, Bunt A, Johanson G. 1977 Orthograde and retrograde axoplasmic transport during acute ocular hypertension in the monkey. *Invest. Ophthalmol. Vis. Sci.* **16**, 426–441.
5. Garcia-Valenzuela E, Shareef S, Walsh J, Sharma S. 1995 Programmed cell death of retinal ganglion cells during experimental glaucoma. *Exp. Eye Res.* **61**, 33–44. (doi:10.1016/S0014-4835(95)80056-5)
6. Quigley HA, Nickells RW, Kerrigan LA, Pease ME, Thibault DJ, Zack DJ. 1995 Retinal ganglion cell death in experimental glaucoma and after axotomy occurs by apoptosis. *Invest. Ophthalmol. Vis. Sci.* **36**, 774–786.

7. Quigley HA, Addicks EM, Green WR, Maumenee AE. 1981 Optic nerve damage in human glaucoma. II. The site of injury and susceptibility to damage. *Arch. Ophthalmol*. **99**, 635–649. (doi:10.1001/archopht.1981.03930010635009)
8. Burgoyne CF, Downs JC, Bellezza AJ, Suh JKF, Hart RT. 2005 The optic nerve head as a biomechanical structure: a new paradigm for understanding the role of IOP-related stress and strain in the pathophysiology of glaucomatous optic nerve head damage. *Prog. Retin. Eye Res*. **24**, 39–73. (doi:10.1016/j.preteyeres.2004.06.001)
9. Fechtner RD, Weinreb RN. 1994 Mechanisms of optic nerve damage in primary open angle glaucoma. *Surv. Ophthalmol*. **39**, 23–42. (doi:10.1016/S0039-6257(05)80042-6)
10. Bengtsson B. 1981 The prevalence of glaucoma. *Br. J. Ophthalmol*. **65**, 46–49. (doi:10.1136/bjo.65.1.46)
11. Sommer A, Tielsch JM, Katz J, Quigley HA, Gottsch JD, Javitt J, Singh K. 1991 Relationship between intraocular pressure and primary open angle glaucoma among white and black Americans: the Baltimore Eye Survey. *Arch. Ophthalmol*. **109**, 1090–1095. (doi:10.1001/archopht.1991.01080080050026)
12. Atchison DA, Jones CE, Schmid KL, Pritchard N, Pope JM, Strugnell WE, Riley RA. 2004 Eye shape in emmetropia and myopia. *Invest. Ophthalmol. Vis. Sci*. **45**, 3380–3386. (doi:10.1167/iovs.04-0292)
13. Celorio J, Pruett RC. 1991 Prevalence of lattice degeneration and its relation to axial length in severe myopia. *Am. J. Ophthalmol*. **111**, 20–23. (doi:10.1016/S0002-9394(14)76891-6)
14. Marcus MW, de Vries MM, Montolio FGJ, Jansonius NM. 2011 Myopia as a risk factor for open-angle glaucoma: a systematic review and meta-analysis. *Ophthalmology* **118**, 1989–1994. (doi:10.1016/j.ophtha.2011.03.012)
15. Coudrillier B, Tian J, Alexander S, Myers KM, Quigley HA, Nguyen TD. 2012 Biomechanics of the human posterior sclera: age- and glaucoma-related changes measured using inflation testing. *Invest. Ophthalmol. Vis. Sci*. **53**, 1714–1728. (doi:10.1167/iovs.11-8009)
16. Girard MJ, Suh JKF, Bottlang M, Burgoyne CF, Downs JC. 2011 Biomechanical changes in the sclera of monkey eyes exposed to chronic IOP elevations. *Invest. Ophthalmol. Vis. Sci*. **52**, 5656–5669. (doi:10.1167/iovs.10-6927)
17. Downs JC, Suh J, Thomas KA, Bellezza AJ, Hart RT, Burgoyne CF. 2005 Viscoelastic material properties of the peripapillary sclera in normal and early-glaucoma monkey eyes. *Invest. Ophthalmol. Vis. Sci*. **46**, 540–546. (doi:10.1167/iovs.04-0114)
18. Avetisov E, Savitskaya N, Vinetskaya M, Iomdina E. 1982 A study of biochemical and biomechanical qualities of normal and myopic eye sclera in humans of different age groups. *Metab. Pediatr. Syst. Ophthalmol*. **7**, 183–188.
19. Phillips J, McBrien N. 1995 Form deprivation myopia: elastic properties of sclera. *Ophthal. Physiol. Opt*. **15**, 357–362. (doi:10.1016/0275-5408(95)00062-I)
20. Phillips JR, Khalaj M, McBrien NA. 2000 Induced myopia associated with increased scleral creep in chick and tree shrew eyes. *Invest. Ophthalmol. Vis. Sci*. **41**, 2028–2034.
21. Grytz R, Siegwart JT. 2015 Changing material properties of the tree shrew sclera during minus lens compensation and recovery. *Invest. Ophthalmol. Vis. Sci*. **56**, 2065–2078. (doi:10.1167/iovs.14-15352)
22. Siegwart JT, Norton TT. 1999 Regulation of the mechanical properties of tree shrew sclera by the visual environment. *Vis. Res*. **39**, 387–407. (doi:10.1016/S0042-6989(98)00150-3)
23. Bailey AJ. 1987 Structure, function and ageing of the collagens of the eye. *Eye* **1**, 175–183. (doi:10.1038/eye.1987.34)
24. Rada JAS, Shelton S, Norton TT. 2006 The sclera and myopia. *Exp. Eye Res*. **82**, 185–200. (doi:10.1016/j.exer.2005.08.009)
25. Ayad S, Boot-Handford R, Humphries M, Kadler K, Shuttleworth A. 1994 *The extracellular matrix factsbook*, 2nd edn. London, UK: Academic Press.
26. Breen M, Johnson RL, Sittig R, Weinstein H, Veis A. 1972 The acidic glycosaminoglycans in human fetal development and adult life: cornea, sclera and skin. *Connect. Tissue Res*. **1**, 291–303. (doi:10.3109/03008207209152087)
27. Trier K, Olsen EB, Ammitzbøll T. 1990 Regional glycosaminoglycans composition of the human sclera. *Acta Ophthalmol*. **68**, 304–306. (doi:10.1111/j.1755-3768.1990.tb01926.x)
28. Rada JA, Achen VR, Penugonda S, Schmidt RW, Mount BA. 2000 Proteoglycan composition in the human sclera during growth and aging. *Invest. Ophthalmol. Vis. Sci*. **41**, 1639–1648.
29. Trier K. 2005 The sclera. *Adv. Organ Biol*. **10**, 353–373. (doi:10.1016/S1569-2590(05)10013-5)
30. Comper WD, Laurent TC. 1978 Physiological function of connective tissue polysaccharides. *Physiol. Rev*. **58**, 255–315.
31. Elliott G, Goodfellow J, Woolgar A. 1980 Swelling studies of bovine corneal stroma without bounding membranes. *J. Physiol*. **298**, 453–470. (doi:10.1113/jphysiol.1980.sp013094)
32. Scott JE, Bosworth TR. 1990 A comparative biochemical and ultrastructural study of proteoglycan–collagen interactions in corneal stroma. Functional and metabolic implications. *Biochem. J*. **270**, 491–497. (doi:10.1042/bj2700491)
33. Öbrink B. 1973 A study of the interactions between monomeric tropocollagen and glycosaminoglycans. *Eur. J. Biochem*. **33**, 387–400. (doi:10.1111/j.1432-1033.1973.tb02695.x)
34. Pogany G, Hernandez DJ, Vogel KG. 1994 The *in vitro* interaction of proteoglycans with type I collagen is modulated by phosphate. *Arch. Biochem. Biophys*. **313**, 102–111. (doi:10.1006/abbi.1994.1365)
35. Hedbom E, Heinegård D. 1993 Binding of fibromodulin and decorin to separate sites on fibrillar collagens. *J. Biol. Chem*. **268**, 27 307–27 312.
36. Raspanti M, Viola M, Forlino A, Tenni R, Gruppi C, Tira ME. 2008 Glycosaminoglycans show a specific periodic interaction with type I collagen fibrils. *J. Struct. Biol*. **164**, 134–139. (doi:10.1016/j.jsb.2008.07.001)
37. Scott JE. 1988 Proteoglycan–fibrillar collagen interactions. *Biochem. J*. **252**, 313–323. (doi:10.1042/bj2520313)
38. Maurice DM. 1957 The structure and transparency of the cornea. *J. Physiol*. **136**, 263–286. (doi:10.1113/jphysiol.1957.sp005758)
39. Huang Y, Meek KM. 1999 Swelling studies on the cornea and sclera: the effects of pH and ionic strength. *Biophys. J*. **77**, 1655–1665. (doi:10.1016/S0006-3495(99)77013-X)
40. Borcherding MS, Blacik L, Sittig R, Bizzell JW, Breen M, Weinstein H. 1975 Proteoglycans and collagen fibre organization in human corneoscleral tissue. *Exp. Eye Res*. **21**, 59–70. (doi:10.1016/0014-4835(75)90057-3)
41. Scott J. 1991 Proteoglycan: collagen interactions and corneal ultrastructure. *Biochem. Soc. Trans*. **19**, 877–881. (doi:10.1042/bst0190877)
42. Quigley HA, Dorman-Pease ME, Brown AE. 1991 Quantitative study of collagen and elastin of the optic nerve head and sclera in human and experimental monkey glaucoma. *Curr. Eye Res*. **10**, 877–888. (doi:10.3109/02713689109013884)
43. Pijanka JK, Coudrillier B, Ziegler K, Sorensen T, Meek KM, Nguyen TD, Quigley HA, Boote C. 2012 Quantitative mapping of collagen fiber orientation in non-glaucoma and glaucoma posterior human sclerae. *Invest. Ophthalmol. Vis. Sci*. **53**, 5258–5270. (doi:10.1167/iovs.12-9705)
44. Cone-Kimball E, Nguyen C, Oglesby EN, Pease ME, Steinhart MR, Quigley HA. 2013 Scleral structural alterations associated with chronic experimental intraocular pressure elevation in mice. *Mol. Vis*. **19**, 2023.
45. Quigley HA, Brown A, Dorman-Pease ME. 1991 Alterations in elastin of the optic nerve head in human and experimental glaucoma. *Br. J. Ophthalmol*. **75**, 552–557. (doi:10.1136/bjo.75.9.552)
46. Curtin BJ, Iwamoto T, Renaldo DP. 1979 Normal and staphylomatous sclera of high myopia: an electron microscopic study. *Arch. Ophthalmol*. **97**, 912–915. (doi:10.1001/archopht.1979.01020010470017)
47. Norton TT, Rada JA. 1995 Reduced extracellular matrix in mammalian sclera with induced myopia. *Vis. Res*. **35**, 1271–1281. (doi:10.1016/0042-6989(94)00243-F)
48. McBrien NA, Cornell LM, Gentle A. 2001 Structural and ultrastructural changes to the sclera in a mammalian model of high myopia. *Invest. Ophthalmol. Vis. Sci*. **42**, 2179–2187.
49. Knepper PA, Goossens W, Hvizd M, Palmberg PF. 1996 Glycosaminoglycans of the human trabecular meshwork in primary open-angle glaucoma. *Invest. Ophthalmol. Vis. Sci*. **37**, 1360–1367.
50. Tezel G, Edward DP, Wax MB. 1999 Serum autoantibodies to optic nerve head glycosaminoglycans in patients with glaucoma. *Arch. Ophthalmol*. **117**, 917–924. (doi:10.1001/archopht.117.7.917)

51. Fukuchi T, Sawaguchi S, Yue BJ, Iwata K, Hara H, Kaiya T. 1994 Sulfated proteoglycans in the lamina cribrosa of normal monkey eyes and monkey eyes with laser-induced glaucoma. *Exp. Eye Res*. **58**, 231–244. (doi:10.1006/exer.1994.1012)
52. Johnson EC, Morrison JC, Farrell S, Deppmeier L, Moore C, McGinty M. 1996 The effect of chronically elevated intraocular pressure on the rat optic nerve head extracellular matrix. *Exp. Eye Res*. **62**, 663–674. (doi:10.1006/exer.1996.0077)
53. Schmidt MB, Mow VC, Chun LE, Eyre DR. 1990 Effects of proteoglycan extraction on the tensile behavior of articular cartilage. *J. Orthop. Res*. **8**, 353–363. (doi:10.1002/jor.1100080307)
54. Hoffman A, Grande L, Park J. 1976 Sequential enzymolysis of human aorta and resultant stress–strain behavior. *Biomater. Med. Devices Artif. Organs* **5**, 121–145.
55. Eckert CE, Fan R, Mikulis B, Barron M, Carruthers CA, Friebe VM, Vyavahara NR, Sacks MS. 2013 On the biomechanical role of glycosaminoglycans in the aortic heart valve leaflet. *Acta Biomater*. **9**, 4653–4660. (doi:10.1016/j.actbio.2012.09.031)
56. Lujan TJ, Underwood CJ, Henninger HB, Thompson BM, Weiss JA. 2007 Effect of dermatan sulfate glycosaminoglycans on the quasi-static material properties of the human medial collateral ligament. *J. Orthop. Res*. **25**, 894–903. (doi:10.1002/jor.20351)
57. Lujan TJ, Underwood CJ, Jacobs NT, Weiss JA. 2009 Contribution of glycosaminoglycans to viscoelastic tensile behavior of human ligament. *J. Appl. Physiol*. **106**, 423–431. (doi:10.1152/japplphysiol.90748.2008)
58. Gandley R, McLaughlin M, Koob T, Little S, McGuffee L. 1997 Contribution of chondroitin-dermatan sulfate-containing proteoglycans to the function of rat mesenteric arteries. *Am. J. Physiol. Heart Circ. Physiol*. **273**, H952–H960.
59. Al Jamal R, Roughley PJ, Ludwig MS. 2001 Effect of glycosaminoglycan degradation on lung tissue viscoelasticity. *Am. J. Physiol. Lung Cell. Mol. Physiol*. **280**, L306–L315.
60. Hoffman A, Park J, Abrahamson J. 1973 Sequential enzymolysis of ligament and resultant stress–strain behavior. *Biomater. Med. Devices Artif. Organs* **1**, 453–467. (doi:10.3109/10731197309118556)
61. Fessel G, Snedeker JG. 2011 Equivalent stiffness after glycosaminoglycan depletion in tendon—an ultra-structural finite element model and corresponding experiments. *J. Theor. Biol*. **268**, 77–83. (doi:10.1016/j.jtbi.2010.10.007)
62. Murienne BJ, Jefferys JL, Quigley HA, Nguyen TD. 2015 The effects of glycosaminoglycan degradation on the mechanical behavior of the posterior porcine sclera. *Acta Biomater*. **12**, 195–206. (doi:10.1016/j.actbio.2014.10.033)
63. Boubriak O, Urban J, Bron A. 2003 Differential effects of aging on transport properties of anterior and posterior human sclera. *Exp. Eye Res*. **76**, 701–713. (doi:10.1016/S0014-4835(03)00053-8)
64. Tonge TK, Murienne BJ, Coudrillier B, Alexander S, Rothkopf W, Nguyen TD. 2013 Minimal preconditioning effects observed for inflation tests of planar tissues. *J. Biomech. Eng*. **135**, 114502. (doi:10.1115/1.4025105)
65. Girard MJ, Downs JC, Bottlang M, Burgoyne CF, Suh JKF. 2009 Peripapillary and posterior scleral mechanics—Part II: Experimental and inverse finite element characterization. *J. Biomech. Eng*. **131**, 051012. (doi:10.1115/1.3113683)
66. Genovese K. 2009 A video-optical system for time-resolved whole-body measurement on vascular segments. *Opt. Lasers Eng*. **47**, 995–1008. (doi:10.1016/j.optlaseng.2009.04.017)
67. Schultz DS, Lotz JC, Lee SM, Trinidad ML, Stewart JM. 2008 Structural factors that mediate scleral stiffness. *Invest. Ophthalmol. Vis. Sci*. **49**, 4232–4236. (doi:10.1167/iovs.08-1970)
68. Norman RE, Flanagan JG, Rausch SM, Sigal IA, Tertinegg I, Eilaghi A, Portnoy S, Sled JG, Ethier CR. 2010 Dimensions of the human sclera: thickness measurement and regional changes with axial length. *Exp. Eye Res*. **90**, 277–284. (doi:10.1016/j.exer.2009.11.001)
69. Vurgese S, Panda-Jonas S, Jonas JB. 2012 Scleral thickness in human eyes. *PLoS ONE* **7**, e29692. (doi:10.1371/journal.pone.0029692)
70. Hedbys BO. 1961 The role of polysaccharides in corneal swelling. *Exp. Eye Res*. **1**, 81–91. (doi:10.1016/S0014-4835(61)80012-2)
71. Pereira P, Bedran-de Castro A, Duarte W, Yamauchi M. 2007 Removal of noncollagenous components affects dentin bonding. *J. Biomed. Mater. Res. B Appl. Biomater*. **80**, 86–91. (doi:10.1002/jbm.b.30572)
72. Quacci D, Dell'Orbo C, Diaz G. 1992 Collagen fibril ultrastructure alters after glycanolytic digestion. *Ann. Anat*. **174**, 569–574. (doi:10.1016/S0940-9602(11)80324-9)
73. Danielson KG, Baribault H, Holmes DF, Graham H, Kadler KE, Iozzo RV. 1997 Targeted disruption of decorin leads to abnormal collagen fibril morphology and skin fragility. *J. Cell Biol*. **136**, 729–743. (doi:10.1083/jcb.136.3.729)
74. Corsi A *et al.* 2002 Phenotypic effects of biglycan deficiency are linked to collagen fibril abnormalities, are synergized by decorin deficiency, and mimic Ehlers–Danlos-like changes in bone and other connective tissues. *J. Bone Miner. Res*. **17**, 1180–1189. (doi:10.1359/jbmr.2002.17.7.1180)